Inverse Cascade Spectrum of Gravity Waves in the Presence of a Condensate: A Direct Numerical Simulation

Alexander O. Korotkevich[*]

Department of Mathematics and Statistics, University of New Mexico,
MSC01 1115, 1 University of New Mexico, Albuquerque, New Mexico 87131-0001, USA
and L.D. Landau Institute for Theoretical Physics RAS, Prospekt Akademika Semenova 1A,
Chernogolovka, Moscow region, 142432, Russian Federation

During the set of direct numerical simulations of the forced isotropic turbulence of surface gravity waves in the framework of primordial dynamical equations, the universal inverse cascade spectrum was observed. The slope of the spectrum is the same (in the margin of error) for different levels of pumping and nonlinearity as well as dissipation present in the system. In all simulation runs formation of the inverse cascade spectrum was accompanied by the appearance of a strong long wave background (condensate). The observed slope of the spectrum $\sim k^{-3.07}$ is different from the constant wave action flux solution predicted by the wave turbulence theory $\sim k^{-23/6}$.

Introduction.—The waves turbulence theory (WTT) (see, e.g., Refs. [1,2]) describes the evolution of a distribution function for weakly nonlinear waves. One of the most important applications of WTT is wave forecasting: a statistical description of evolution of the wave field in a sea or an ocean. Most of the current operational wave forecasting models are based either directly on Hasselmann waves kinetic equation [3] (WKE) for surface gravity waves (when one neglects capillary effects) with extra phenomenological terms or on its variations [4,5]. Thus, verification of the applicability of WKE for different setups is an important practical question. Two constant flux solutions of WKE for gravity waves, corresponding to direct [6] and inverse [7] cascades, were found by Zakharov and coauthors [1,2,8]. These Kolmogorov-Zakharov (KZ) solutions are formulated for inertial intervals: ranges of scales where dynamics is determined by the nonlinear interaction of waves, and direct influence of dissipation or pumping is negligible. If one could confirm the observation of these solutions in a field, laboratory, or numerical experiment, this would be a strong argument in support of the applicability of WKE in particular conditions.

While the spectrum corresponding to the direct cascade of energy to small scales was observed both experimentally [9,10] and numerically [11–15], the inverse cascade spectrum of wave action from smaller to larger scales appeared to be a harder case. Although frequency downshift, which can be explained by inverse cascade, was observed in direct numerical simulations (DNSs) of decaying turbulence (evolution of initial spectrum without forcing in the system) [11,16–18], it could not be a substitute for the inverse

cascade spectrum, which can be obtained only in the case of forced turbulence. Perhaps, the first attempt toward this goal was Ref. [19], where the initial stage of the formation of the KZ-spectrum was demonstrated, but the range of scales with a powerlike spectrum was not sufficient to determine the slope. The attempt to observe both inverse and direct cascades simultaneously [20] has resulted in the formation of an inverse cascade and a *condensate* (strong long wave background), which affected even the direct cascade spectrum, but the range of scales in the inverse cascade region was again insufficient to determine the slope accurately enough. A description of some of the laboratory experiments, where an observation of inverse cascade was attempted, can be found in Ref. [21]. The major problem in early attempts [22] was the small size of the basin which required one to excite waves in the capillary-gravity crossover region [23]. Even in later experiments in a relatively large wave tank [24], both the dynamical range and finite size effects prevented clear observation of the slope of the inverse cascade. In all numerical and at least some of the laboratory experiments mentioned above formation of the condensate was observed (although, not always noted).

The importance of condensate influence upon the gravity waves spectrum was demonstrated in Ref. [20] and investigated in details in Ref. [25]. At least one of the important mechanisms of the condensate formation is the arrest of the nonlinear interactions due to discreteness of the homogeneous wave numbers grid, typical for both DNS with periodic boundary conditions and relatively small laboratory basins, like in Ref. [22]; thus the condensate is not

purely a numerical artifact. The importance of discreteness of the wave numbers grid for nonlinear interactions was noted a long time ago for waves in resonators [26,27] and investigated in detail with direct application to WTT [15,28–30]. Although there are exact resonances present on a discrete homogeneous grid of wave vectors [31], the quasiresonances due to nonlinear broadening of the resonance curve play a very important role for turbulent fluxes in simulations of WTT [32]. As the inverse cascade spectrum propagates further from the pumping region to the smaller wave numbers (larger scales), eventually nonlinear interaction through quasiresonances is arrested by the discreteness and the flux only brings wave action without further propagation, resulting in the accumulation of it at some large scale [20,25,33] (a similar phenomenon was observed for direct cascade in Ref. [34]). This results in the formation of a strong (an order of magnitude larger than even closest harmonics) long wave background, which we call condensate. The powerlike inverse cascade spectrum can be observed in the inertial interval between condensate and pumping regions, like in laboratory experiments [21,22] or in DNS [19,20]. In these simulations the inertial interval was too short to allow one to determine the slope of the inverse cascade with reasonable accuracy and compare it with the WTT prediction. Taking into account the extremely slow formation of the inverse cascade (meaning a smaller resolution for faster computations) and necessity of a reasonable dynamic range for determining the slope of the spectrum, one needs to find a compromise between these contradicting requirements.

In this Letter we present results of DNSs in the framework of primordial dynamical equations of the forced turbulence of surface gravity waves and formation of the inverse cascade with a powerlike spectrum. Simulations were performed for different levels of pumping, resulting in different nonlinearity levels and different parameters of dissipation, for an extremely long ($\approx 10^6$ periods of central pumping harmonic) period of time. In all the cases we obtained condensate formation and were able to determine the slope of the inverse cascade spectrum, virtually the same for all simulations, yet different from one predicted by WTT. The new spectrum is simultaneously a challenge for WTT, a more detailed set of data supporting some experiments, and a stimulus for new breakthroughs in theory.

Problem formulation.—We consider a potential flow (velocity of the fluid is $\mathbf{v} = \nabla \Phi$) of an ideal incompressible fluid of infinite depth. Elevation of the 2D surface over 3D fluid from the steady state is described by a function $\eta(\mathbf{r}; t)$, where $\mathbf{r} = (x, y)^T$ is the coordinate vector in a horizontal plane. The velocity potential on the surface is $\psi(\mathbf{r}; t) = \Phi|_{z=\eta(\mathbf{r};t)}$. The system is Hamiltonian [35] with respect to variables η and ψ. An average slope of the surface $\mu = \sqrt{\langle |\nabla \eta(\mathbf{r})|^2 \rangle}$, also called steepness, in most of the observations is a small parameter $\mu \ll 1$. One can expand

the Hamiltonian in powers of μ (see Sec. I of the Supplemental Material [36]) and obtain Hamiltonian equations:

$$\dot{\eta} = \hat{k}\psi - [\nabla(\eta\nabla\psi)] - \hat{k}[\eta\hat{k}\psi]$$
$$+ \hat{k}(\eta\hat{k}[\eta\hat{k}\psi]) + \frac{1}{2}\Delta[\eta^2\hat{k}\psi] + \frac{1}{2}\hat{k}[\eta^2\Delta\psi] - F^{-1}[\gamma_k\eta_k],$$
$$\dot{\psi} = -g\eta - \frac{1}{2}[(\nabla\psi)^2 - (\hat{k}\psi)^2]$$
$$- [\hat{k}\psi]\hat{k}[\eta\hat{k}\psi] - [\eta\hat{k}\psi]\Delta\psi - F^{-1}[\gamma_k\psi_\mathbf{k}] + F^{-1}[f_k]. \quad (1)$$

Artificial pumping and damping terms will be described later in Eq. (5). Here $\hat{k}$ is a linear integral operator $\hat{k} = \sqrt{-\Delta}$, such that $\hat{k}f_\mathbf{r}$ in k space corresponds to multiplication of Fourier (in the horizontal XY plane) coefficients $f_\mathbf{k}$:

$$\hat{F}[f_\mathbf{r}] = f_\mathbf{k} = \frac{1}{L_x L_y} \int_0^{L_x} \int_0^{L_y} f_\mathbf{r} e^{-i\mathbf{k}\mathbf{r}} d\mathbf{r},$$
$$\hat{F}^{-1}[f_\mathbf{k}] = f_\mathbf{r} = \sum_\mathbf{k} f_\mathbf{k} e^{i\mathbf{k}\mathbf{r}}$$

by $k = |\mathbf{k}| = \sqrt{k_x^2 + k_y^2}$. For gravity waves these reduced Hamiltonian equations describe four-wave interaction. In the case of a statistical description of the wave field, WKE for the distribution of wave action $n(k, t) = \langle |a_\mathbf{k}(t)|^2 \rangle$ is used. Here

$$a_\mathbf{k} = \sqrt{\omega_k/(2k)}\eta_\mathbf{k} + i\sqrt{k/(2\omega_k)}\psi_\mathbf{k}, \quad (2)$$

are complex normal variables. For gravity waves $\omega_k = \sqrt{gk}$. More precisely, one has to use a different function $b_\mathbf{k}$ after canonical transformation eliminating nonresonant cubic terms [1,2] in the Hamiltonian, but the relative difference between corresponding n_k's in the case of $\mu \approx 0.1$ is of the order of a few percent, so we shall limit ourselves by a simpler function [Eq. (2)].

From WTT [1,2], in the case of four-wave interaction (typical for surface gravity waves), besides equipartion spectra, under few reasonable assumptions, one can find two constant flux KZ solutions [6,7,37] of WKE:

$$n_k^{(1)} = C_1 P^{1/3} k^{-\frac{2\beta}{3}-d}, \qquad n_k^{(2)} = C_2 Q^{1/3} k^{-\frac{2\beta-\delta}{3}-d}. \quad (3)$$

For surface gravity waves, a coefficient of homogeneity of nonlinear interaction coefficient $\beta = 3$, the power of dispersion law $\delta = 1/2$, and the dimension of the surface $d = 2$. As a result we get

$$n_k^{(1)} = C_1 P^{1/3} k^{-4}, \qquad n_k^{(2)} = C_2 Q^{1/3} k^{-23/6}. \quad (4)$$

The solution $n_k^{(1)}$ describes a direct cascade of energy from large pumping to small dissipative scales and was observed

in simulations [11–13,20]. The second spectrum $n_k^{(2)}$ describes an inverse cascade of wave action from small pumping to larger scales.

Numerical scheme parameters.—We simulate Eq. (1) in a (double) periodic box $L_x = L_y = 2\pi$. Grid resolution $N_x = N_y = 512$.

Pumping on large scales [term with f_k in Eq. (1)] and dissipation on small scales (terms with γ_k) are

$$f_k = 4F_0 e^{iR_{\mathbf{k}}(t)} \frac{(k - k_{p1})(k_{p2} - k)}{(k_{p2} - k_{p1})^2};$$

$$\gamma_k = \begin{cases} \gamma_0 (k - k_d)^2, & k \geq k_d, \\ \gamma_k = 0, & k < k_d. \end{cases} \qquad (5)$$

The pumping parameters $F_0 = 5 \times 10^{-9} (\times 2, \times 4, \times 8)$, $k_{p1} = 60$, and $k_{p2} = 64$, i.e., for four different simulation runs the amplitude $|F_0|$ was differing by factors $\times 2$, $\times 4$, and $\times 8$ from the smallest one. Function f_k is a parabola with zeros at k_{p1} and k_{p2} and extremum equal to $|F_0|$ in the middle $k_p = 62$ between them; f_k is zero outside of an interval $k \in [k_{p1}; k_{p2}]$. $R_{\mathbf{k}}(t)$ is a uniformly distributed random number in the interval $(0, 2\pi]$, different for every harmonic and time step. Initial amplitudes for all $\eta_{\mathbf{k}}$ and $\psi_{\mathbf{k}}$ harmonics were 10^{-12}, and all phases were uniformly distributed random numbers between $(0, 2\pi]$. Damping starts at $k_d = 128$ and zero for larger scales (to avoid the influence of aliasing due to cubic nonlinearity in our equations, we suppress harmonics with $k > k_{\mathrm{max}}/2$, where $k_{\mathrm{max}} = 256$). Following Ref. [38] damping has to be included in both equations of Eq. (1). The value of γ_0 was chosen automatically to ensure 6 orders of harmonics magnitude difference between the center of the pumping region $k_p = 62$ and the last Fourier harmonics at $k = k_{\mathrm{max}}$. It guarantees good quality of the solution in spite of the fact that the Fourier series is being truncated. Later, after formation of the condensate, the difference of the largest and smallest (in magnitude) harmonics reaches 7 orders of magnitude. It should be noted, that the values of γ_0 were different for different levels of pumping as different fluxes of energy to the high k's had to be dissipated. Details of the numerical algorithm can be found in Ref. [30]. FFTW library [39] was used as a discrete Fourier transform implementation.

In the k-space supports of γ_k and f_k are separated by the inertial interval, where the KZ solution corresponding to the direct cascade of energy could be recognized, but the range of scales in this set of numerical simulations was insufficient. Another inertial interval is located between $k = 0$ and the pumping region; here we expected to observe inverse cascade. Because both dissipation and pumping are isotropic (except for random phases) with respect to the polar angle, we expect the same property for a solution, and we use it for averaging the resulting spectra to replace ensemble averaging.

Computations were performed on a designated CPU core for each value of F_0 and took more than a year. This is the reason for a relatively small grid resolution, even with respect to our previous computations [13,20,25]. During previous works it had become clear that formation of the inverse cascade is an extremely slow process, which is explained by the fact that the interaction coefficient for gravity waves behaves as $\sim k^3$, which means that interaction slows quickly with a decrease of k. Also, in weakly nonlinear approximation characteristic nonlinear time T_{nl}, when nonlinearity shows itself (amplitude change of order 1), has to be much more than a period corresponding to linear dispersion $T_k = 2\pi/\omega_k$, while linear frequency ω_k also decays with a decrease of k. In order to avoid a direct drain of energy from the pumping region through slave harmonics, we had to ensure that only third harmonic $(3k_{p2})$ of pumping is in the dissipation region (see Ref. [40]). Simultaneously, we had to leave room for inverse cascade development. Taking into account all these considerations and the enormous time of the inverse cascade formation (we had to compute till times $> 10^6 T_p$, where $T_p = 2\pi/\omega_{k_p}$), the relatively small resolution 512×512 was a reasonable compromise.

Numerical results.—The computations were performed until a time close to a million of periods of a harmonic at the maximum of pumping T_p. As a replacement of ensemble averaging, which is unfeasible taking into account the computation time, in order to compute $n_k = \langle |a_k|^2 \rangle$ we used averaging over an angle as the situation is isotropic and pumping has a random phase in every harmonics and at every moment of time. There are more harmonics to average over in larger k's, meaning fewer fluctuations of $\langle |a_k|^2 \rangle$. The resulting mean steepnesses μ for all four cases were 0.054, 0.067, 0.093, and 0.135. It should be noted that these values correspond to a very different dissipation due to nonlinear processes, as was shown in Refs. [41,42] (see Ref. [43]). The obtained angle averaged spectra are shown
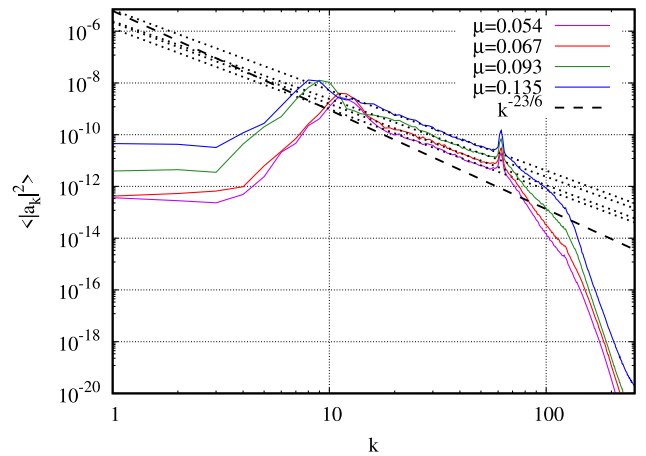

FIG. 1. All simulation spectra (solid lines) with corresponding least squares fits (dotted lines, values of slopes are given in Table I) and KZ-spectrum slope (dashed line).
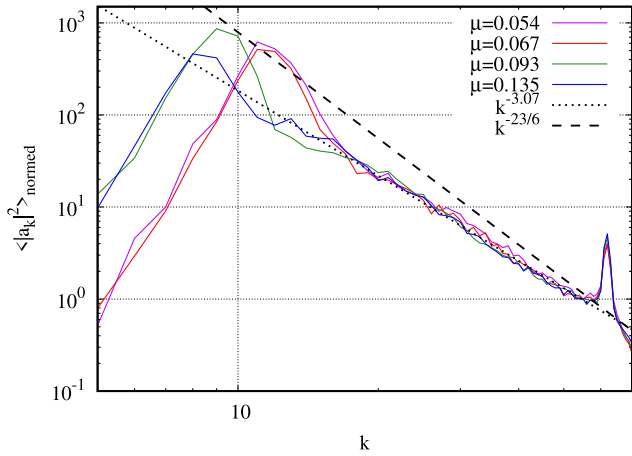
FIG. 2. All simulation spectra (solid lines) normed to have a value of $\langle |a_k|^2 \rangle$ at $k = 55$ to be 1 with a least squares fits (dotted line; value of the slope is given in Table I) over data points between condensate and pumping regions for all spectra and KZ-spectrum slope (dashed line).

in Fig. 1. In accordance with the theory in Ref. [30], the width of the resonant curve, necessary for working quasiresonances, depends on the nonlinearity in the system, resulting in further propagation of the inverse cascade and condensate for higher levels of steepness. For scales between regions influenced by condensate and pumping, we observe powerlike spectra (shown by dotted lines), with slopes practically independent of steepness. As one can see from Fig. 1, the higher the nonlinearity level is, the longer the inertial interval is, where a powerlike spectrum can be observed. This universal spectrum has a slope which is even visually different from the KZ spectrum $\sim k^{-23/6} \approx k^{-3.83}$. The slopes' values together with intervals used for linear least squares fit (in double logarithmic representation, like in Fig. 1) are given in Table I. The least squares fit was performed both in the OCTAVE [44] (part of GNU PROJECT [45]) package (via standard QR approach) and in GNUPLOT [46] (via Marquardt-Levenberg algorithm); standard errors [47] are from the Gnuplot computations. The slopes are significantly different from $-23/6 \approx -3.83$ in accordance

TABLE I. Least squares fits for different simulation spectra. The second column shows the range of k between the condensate and pumping influenced regions; the third column gives the average slope α for $\langle |a_k|^2 \rangle \sim k^\alpha$; the last column shows an estimated error of the fit.

μ	$k \in$	Average slope	Slope error
0.054	[17;55]	−3.12	±0.04
0.067	[16;55]	−3.14	±0.05
0.093	[12;56]	−3.01	±0.05
0.135	[11;56]	−3.11	±0.04
All	170 points	−3.07	±0.02

with Fig. 1. To better understand the universality of the observed inverse cascade spectrum, we normalized all results in order to make an amplitude of $|a_k|^2$ of the harmonic $k = 55$ (see Ref. [48]) equal to 1. As a result, all spectra collapsed to a single curve (line) in the inertial interval (up to fluctuations due to insufficient averaging), shown in Fig. 2. We used the set of all available points in inertial intervals for all simulation runs for a least squares fit. The resulting slope is given in the last line of Table I and shown as a dotted line in Fig. 2. The value of the estimated spectrum slope is $\langle |a_k|^2 \rangle \sim k^{-3.07}$, which is again, expectedly, different from the one predicted by WTT [see Eq. (4)]. The reason for this inconsistency is yet to be found (e.g., see Ref. [49]).

It also can be noted that Fig. 2 strongly resembles Fig. 3 in Ref. [19], with the difference that we performed four different simulations and have a significantly longer inertial interval for inverse cascade allowing us to determine the slope with reasonable accuracy. The slopes in Table I with given errors margins have a point of intersection for all but one simulation runs (see Ref. [52]), corresponding to the slope −3.09. Thus, one can conclude that the slope is roughly between −3.0 and −3.1, and probably closer to the −3.1 value. Nevertheless, the difference between observed slope and the one predicted by WTT is clear both visually and numerically.

Conclusion.—During four numerical simulations with different pumping and dissipation parameters, we observed the formation of the inverse cascade and the condensate. In the inertial interval between condensate and pumping regions the universal spectrum is close to a powerlike function with a least square fit suggesting $\sim k^{-3.07}$ slope. This is close to an experimentally observed spectrum in recent wave tank experiments [21] (see Fig. 12 (right) where our $n_k \sim k^{-3.07}$ would correspond to $E_k \sim k^{-1.57}$, close to the $E_k \sim k^{-1.5}$ proposed in that work), especially taking into account relatively noisy experimental data and a short range of scales. The slope of the spectrum is virtually identical for dramatically different levels of nonlinearity, which suggests the universality of the observed solution. Regardless of the fact that the spectrum is significantly different from the one predicted by WTT, the dependence of a constant in front of the powerlike function on the pumping parameters was investigated (see Sec. II of the Supplemental Material [36]). It was shown that at least in the first (linear) approximation the dependence of the constant on the flux is in reasonable agreement with Eq. (4), namely with $Q^{1/3}$, which hints that the new spectrum is a result of four-wave interaction.

The applicability of WKE (which is derived for an infinite domain) to DNS in a periodic box is yet to be investigated in detail. Recent works on the 3D nonlinear Schrödinger equation (NLSE) [53] and 1D quintic NLSE [54] give us hope that a precise range of simulation parameters, when one could expect quantitative

correspondence between WKE and DNS of dynamical equations for surface gravity waves, will be determined in future works. For now we could use previous simulations [11,13,17,20,32] as empirical evidence that one could expect at least qualitative correspondence (spectra slopes, spectrum peak downshift, etc.) for simulations in the frameworks of these significantly different models.

The constant wave action flux KZ spectrum $\sim k^{-23/6}$ was derived for a particular case (infinite inertial interval, one spectrum in the whole range of wave numbers, etc.), which is different from what we observe in our simulations and experiments (finite range of scales, limited both by condensate and pumping). Similarly, the direct cascade of the energy KZ spectrum was not always observed in wave tank experiments [55,56], while in the open water in most of the cases [9,10] the KZ spectrum is observed. An explanation of the spectrum reported in this Letter is yet to be proposed, although previous works [20,25,33] hint that the condensate plays a major role for processes in the inverse cascade inertial interval. In order to take into account the condensate, one could use several different approaches: Bogolyubov transformation, similar to the technique used in a recent work [57]; taking into account the bottleneck phenomenon as was done in Ref. [58] for 2D turbulence; subtracting the condensate as in Refs. [59,60]; and studying the spectrum of remaining fluctuations. A lot depends on the type of the condensate. If it is a coherent structure, the approaches listed above could be applied. As the condensate is a ring with a radius between 8 and 15 for different simulations with a width around several harmonics, the total number of discrete harmonics in condensate is more than 100, and if they are stochastic enough (this is yet to be defined) the situation could be described by WKE [61]. In all of these cases complexity of the interaction coefficient (e.g., see Appendix B in Ref. [62]) for surface gravity waves makes analysis difficult enough to be a topic of a separate investigation. The final $\eta(\mathbf{r})$ and $\psi(\mathbf{r})$ surfaces for all four runs can be downloaded in the Supplemental Material [36]. Description of the file format is given in Sec. III of the Supplemental Material [36].

---

*alexkor@math.unm.edu

[1] V. E. Zakharov, V. S. Lvov, and G. Falkovich, *Kolmogorov Spectra of Turbulence I* (Springer-Verlag, Berlin, 1992).

[2] S. V. Nazarenko, *Wave Turbulence* (Springer-Verlag, Berlin Heidelberg, 2011).

[3] K. Hasselmann, J. Fluid Mech. **12**, 481 (1962).

[4] G. J. Komen, L. Cavaleri, M. Donelan, K. Hasselmann, and P. A. E. M. Janssen, *Dynamics and Modelling of Ocean Waves* (Cambridge University Press, Cambridge, UK, 1994).

[5] L. Cavaleri *et al.*, Progr. Oceanogr. **75**, 603 (2007).

[6] V. E. Zakharov and N. N. Filonenko, Sov. Phys. Dokl. **11**, 881 (1967).

[7] M. M. Zaslavskii and V. E. Zakharov, Izv. Akad. Nauk SSSR Fiz. Atm. i Okeana **18**, 747 (1982).

[8] V. E. Zakharov, in *Breaking Waves*, edited by M. L. Banner and R. H. J. Grimshaw (Springer Berlin Heidelberg, Berlin, Heidelberg, 1992) pp. 69–91.

[9] M. A. Donelan, J. Hamilton, and W. H. Hui, Phil. Trans. R. Soc. A **315**, 509 (1985).

[10] P. A. Hwang, D. W. Wang, E. J. Walsh, W. B. Krabill, and R. N. Swift, J. Phys. Oceanogr. **30**, 2753 (2000).

[11] M. Onorato, A. R. Osborne, M. Serio, D. Resio, A. Pushkarev, V. E. Zakharov, and C. Brandini, Phys. Rev. Lett. **89**, 144501 (2002).

[12] A. I. Dyachenko, A. O. Korotkevich, and V. E. Zakharov, JETP Lett. **77**, 546 (2003).

[13] A. I. Dyachenko, A. O. Korotkevich, and V. E. Zakharov, Phys. Rev. Lett. **92**, 134501 (2004).

[14] N. Yokoyama, J. Fluid Mech. **501**, 169 (2004).

[15] Y. Lvov, S. V. Nazarenko, and B. Pokorni, Physica (Amsterdam) **218D**, 24 (2006).

[16] V. E. Zakharov, A. O. Korotkevich, A. Pushkarev, and A. I. Dyachenko, JETP Lett. **82**, 487 (2005).

[17] V. E. Zakharov, A. O. Korotkevich, A. Pushkarev, and D. Resio, Phys. Rev. Lett. **99**, 164501 (2007).

[18] A. O. Korotkevich, A. Pushkarev, D. Resio, and V. E. Zakharov, Eur. J. Mech. B **27**, 361 (2008).

[19] S. Y. Annenkov and V. I. Shrira, Phys. Rev. Lett. **96**, 204501 (2006).

[20] A. O. Korotkevich, Phys. Rev. Lett. **101**, 074504 (2008).

[21] S. Nazarenko and S. Lukaschuk, Annu. Rev. Condens. Matter Phys. **7**, 61 (2016).

[22] L. Deike, C. Laroche, and E. Falcon, Europhys. Lett. **96**, 34004 (2011).

[23] E. Falcon and N. Mordant, Annu. Rev. Fluid Mech. **54**, 1 (2022).

[24] E. Falcon, G. Michel, G. Prabhudesai, A. Cazaubiel, M. Berhanu, N. Mordant, S. Aumaître, and F. Bonnefoy, Phys. Rev. Lett. **125**, 134501 (2020).

[25] A. O. Korotkevich, Math. Comput. Simul. **82**, 1228 (2012).

[26] E. A. Kartashova, Physica (Amsterdam) **54D**, 125 (1991).

[27] E. Kartashova, Europhys. Lett. **97**, 30004 (2012).

[28] A. I. Dyachenko, A. O. Korotkevich, and V. E. Zakharov, JETP Lett. **77**, 477 (2003).

[29] S. V. Nazarenko, J. Stat. Mech. (2006) L02002.

[30] A. O. Korotkevich, A. I. Dyachenko, and V. E. Zakharov, Physica (Amsterdam) **321-322D**, 51 (2016).

[31] Z. Zhang and Y. Pan, Phys. Rev. E **106**, 044213 (2022).

[32] S. Y. Annenkov and V. I. Shrira, J. Fluid Mech. **561**, 181 (2006).

[33] A. O. Korotkevich, JETP Lett. **97**, 126 (2013).

[34] T. Y. Sheffield and B. Rumpf, Phys. Rev. E **95**, 062225 (2017).

[35] V. E. Zakharov, J. Appl. Mech. Tech. Phys. **9**, 190 (1968).

[36] See Supplemental Material at http://link.aps.org/supplemental/10.1103/PhysRevLett.130.264002 for a complete derivation of weakly nonlinear dynamical Hamiltonian equations for surface gravity waves over 3D ideal incompressible fluid; detailed information about the dependence of the constant in front of the proposed spectrum on the forcing amplitude; description of the final $\eta-$ and ψ-surfaces files for all of the simulation runs.

[37] V. E. Zakharov, On the theory of surface waves, Ph.D. thesis, Budker Institute for Nuclear Physics, Novosibirsk, USSR, 1967.

[38] F. Dias, A. I. Dyachenko, and V. E. Zakharov, Phys. Lett. A **372**, 1297 (2008).

[39] M. Frigo and S. G. Johnson, Proc. IEEE **93**, 216 (2005).

[40] Otherwise the level of pumping and fluxes would strongly depend on the level of dissipation. Importance of such a mechanism was demonstrated in Refs. [17,18].

[41] V. E. Zakharov, A. O. Korotkevich, and A. O. Prokofiev, AIP Proc. **CP1168 2**, 1229 (2009).

[42] A. O. Korotkevich, A. O. Prokofiev, and V. E. Zakharov, JETP Lett. **109**, 309 (2019).

[43] If we would have a large enough dynamical range for development of a direct cascade, according to Ref. [20], it would result in different slopes for the direct cascade spectrum.

[44] GNU Octave, Scientific Programming Language, https://octave.org/ (1988–2022).

[45] GNU Project, http://gnu.org (1984–2022).

[46] Gnuplot, command-driven interactive function plotting program, http://gnuplot.info (1986–2022).

[47] What are standard errors in Gnuplot fit function, http://gnuplot.info/docs_5.5/loc7129.html (1986–2022).

[48] This is the harmonic closest to the region influenced by pumping which is present in all datasets for least square fits in Table I.

[49] One of the factors which might be important is deviation of the dispersion relation from the linear theory in the presence of the condensate (according to Eq. (3), the slope of the inverse cascade spectrum directly depends on the power of dispersion relation δ). It was show in Ref. [33] that in the presence of condensate rotation of phase of harmonics in the inverse cascade region cannot be described with a reasonable accuracy only by linear dispersion relation for gravity waves. One can try to take into account the interaction with condensate, e.g., using Bogolyubov transformation like in the case of dilute Bose gas (see sections about degenerated almost ideal Bose gas in Refs. [50] or [51]).

[50] I. E. D. Aleksey, A. Abrikosov, and Lev P. Gorkov, *Methods of Quantum Field Theory in Statistical Physics* (Fizmatgiz, Moscow, 1962).

[51] E. M. Lifshitz and L. P. Pitaevskii, *Statistical Physics: Course of Theoretical Physics—Vol. 9* (Elsevier, New York, 1978).

[52] Documentation for Gnuplot `fit` function recommends considering standard errors just as an estimation, as many assumptions were used which cannot be justified in our case.

[53] Y. Zhu, B. Semisalov, G. Krstulovic, and S. Nazarenko, Phys. Rev. E **106**, 014205 (2022).

[54] J. W. Banks, T. Buckmaster, A. O. Korotkevich, G. Kovačič, and J. Shatah, Phys. Rev. Lett. **129**, 034101 (2022).

[55] P. Denissenko, S. Lukaschuk, and S. V. Nazarenko, Phys. Rev. Lett. **99**, 014501 (2007).

[56] S. Lukaschuk, S. Nazarenko, S. McLelland, and P. Denissenko, Phys. Rev. Lett. **103**, 044501 (2009).

[57] A. Griffin, G. Krstulovic, V. S. L'vov, and S. Nazarenko, Phys. Rev. Lett. **128**, 224501 (2022).

[58] G. Falkovich, Phys. Fluids **6**, 1411 (1994).

[59] M. Chertkov, C. Connaughton, I. V. Kolokolov, and V. V. Lebedev, Phys. Rev. Lett. **99**, 084501 (2007).

[60] H. Xia, M. Shats, and G. Falkovich, Phys. Fluids **21**, 125101 (2009).

[61] A. O. Korotkevich, S. V. Nazarenko, Y. Pan, and J. Shatah, arXiv:2305.01930.

[62] A. Pushkarev, D. Resio, and V. E. Zakharov, Physica (Amsterdam) **184D**, 29 (2003).

Supplemental material for the paper "Inverse cascade spectrum of gravity waves in the presence of condensate: direct numerical simulation."

Alexander O. Korotkevich*

Department of Mathematics and Statistics, University of New Mexico,
MSC01 1115, 1 University of New Mexico, Albuquerque, NM 87131-0001, USA and
L. D. Landau Institute for Theoretical Physics RAS, Prosp. Akademika Semenova 1A,
Chernogolovka, Moscow region, 142432, Russian Federation
(Dated: March 23, 2023)

In this Supplemental Material we provide a complete derivation of weakly nonlinear dynamical Hamiltonian equations for surface gravity waves over 3D ideal incompressible fluid. We derive it for gravity-capillary waves up to the four-waves interaction terms in the Hamiltonian, which is necessary for gravity waves. Also we provide a as detailed information as currently possible about the dependence of the constant in front of the proposed spectrum on the forcing amplitude.

I. COMPLETE DERIVATION OF WEAKLY NONLINEAR DYNAMICAL EQUATIONS FOR WAVES ON THE SURFACE OF AN IDEAL LIQUID.

A. Exact equations.

1. Laplace equation formulation.

Let us consider three dimensional irrotational flow of an inviscid (ideal) incompressible and homogeneous fluid of infinite depth. Because fluid is irrotational $\mathrm{curl}\mathbf{v} = \mathbf{0}$, we can introduce velocity potential $\Phi = \Phi(x, y, z; t)$ in the following way: $\mathbf{v} = \nabla\Phi$. Because fluid is incompressible $\mathrm{div}\mathbf{v} = 0$ and velocity potential Φ satisfies the Laplace equation

$$\mathrm{div}\mathbf{v} = \Delta\Phi = 0 \tag{1}$$

in the domain filled by fluid

$$-\infty < z < \eta(\mathbf{r}), \quad \mathbf{r} = (x, y). \tag{2}$$

Here and further $\Delta = \nabla^2$ and $\eta = \eta(x, y, t)$ is a fluid surface elevation with respect to a steady state (flat horizontal surface positioned at $z = 0$).

Boundary conditions for velocity potential are as follows

$$\frac{\partial \eta}{\partial t} = \left. \left(\frac{\partial \Phi}{\partial z} - \frac{\partial \Phi}{\partial x}\frac{\partial \eta}{\partial x} - \frac{\partial \Phi}{\partial y}\frac{\partial \eta}{\partial y} \right) \right|_{z=\eta},$$
$$\left. \left(\frac{\partial \Phi}{\partial t} + \frac{1}{2}(\nabla\Phi)^2 \right) \right|_{z=\eta} + p|_{z=\eta} + \rho g\eta = 0, \tag{3}$$
$$p|_{z=\eta} = \sigma\nabla \cdot \frac{\nabla\eta}{\sqrt{1 + (\nabla\eta)^2}}$$

$$\phi_z|_{z \to -\infty} = 0. \tag{4}$$

---

* alexkor@math.unm.edu

Also it is usually reasonable to suppose that all velocities at infinities are zeros as well as surface elevation. We will discuss periodic box case later. Here we introduced gravity acceleration g, fluid density ρ, and surface tension coefficient σ.

2. Hamiltonian equations formulation.

Kinetic and potential energies of the system are the following

$$H = T + U,$$

$$T = \frac{\rho}{2} \int \mathrm{d}^2 r \int_{-\infty}^{\eta} (\nabla\Phi)^2 \mathrm{d}z, \tag{5}$$

$$U = \rho \int \left(\frac{\sigma}{\rho}\left(\sqrt{1 + (\nabla\eta)^2} - 1 \right) + \frac{g}{2}\eta^2 \right) \mathrm{d}^2 r. \tag{6}$$

Let us introduce $\sigma' = \sigma/\rho$, then one can get rid of ρ after renormalization of energies. It will correspond to rescaled time $t \to \rho t$.

System (3), (4) has a Hamiltonian structure. It was shown by Zakharov in 1968 [1] that using variables $\eta(x, y, t)$-surface displacement and velocity potential on the surface $\psi(x, y; t) = \Phi(x, y, \eta(x, y; t); t)$ these boundary conditions take form

$$\frac{\partial \eta}{\partial t} = \frac{\delta H}{\delta \psi}, \quad \frac{\partial \psi}{\partial t} = -\frac{\delta H}{\delta \eta}. \tag{7}$$

Thus variables η, ψ are canonically conjugated.

Kinetic energy cannot be expressed in terms of η, ψ in an explicit form. However, one can find expansion of the Hamiltonian H in powers of nonlinearity. Let use the following vector identity:

$$\nabla\Phi \cdot \nabla\Phi = \mathrm{div}(\Phi\nabla\Phi) - \Phi\Delta\Phi = \mathrm{div}(\Phi\nabla\Phi).$$

Thus, using Stokes' theorem kinetic energy (5) can be rewritten as an integral over the surface:

$$2T = \int (\nabla\Phi)^2 \mathrm{d}V = \int \mathrm{div}(\Phi\nabla\Phi)\mathrm{d}V = \int \Phi\nabla\Phi \cdot \mathrm{d}\mathbf{S}. \quad (8)$$

Here we have to take into account the fact that on infinitely remote boundaries all velocities has to be zeros, thus $\nabla\Phi \equiv \mathbf{0}$ everywhere but on the upper fluid surface. If we consider periodic boundary conditions for x and y, then outgoing flux will be exactly compensated by incoming due to periodicity. So this surface integral has to be understood as an integral over the (upper) surface of the fluid. On the surface radius vector is $\mathbf{R} = x\mathbf{i} + y\mathbf{j} + \eta(x,y)\mathbf{k}$, where $\mathbf{i}$, $\mathbf{j}$, and $\mathbf{k}$ are unit vectors (orts) along directions of x-, y-, and z-axes correspondingly. and for the oriented surface element one can write (we follow an agreement that normal vector is directed outside of the enclosed volume, which for upper surface means that z-component of the normal vector is mostly positive):

$$\mathrm{d}\mathbf{S} = \frac{\partial\mathbf{R}}{\partial x} \times \frac{\partial\mathbf{R}}{\partial y}\mathrm{d}x\mathrm{d}y = \left(\mathbf{k} - \mathbf{i}\frac{\partial\eta}{\partial x} - \mathbf{j}\frac{\partial\eta}{\partial y}\right)\mathrm{d}x\mathrm{d}y.$$

Using this expression of $\mathrm{d}\mathbf{S}$ one can write

$$\begin{aligned} 2T &= \int \Phi\nabla\Phi \cdot \mathrm{d}\mathbf{S} \\ &= \int \Phi\left(\frac{\partial\Phi}{\partial z} - \frac{\partial\Phi}{\partial x}\frac{\partial\eta}{\partial x} - \frac{\partial\Phi}{\partial y}\frac{\partial\eta}{\partial y}\right)\bigg|_{z=\eta} \mathrm{d}x\mathrm{d}y \\ &= \int \Phi\left(\frac{\partial\Phi}{\partial z} - \nabla\Phi \cdot \nabla\eta\right)\bigg|_{z=\eta} \mathrm{d}x\mathrm{d}y \quad (9) \end{aligned}$$

Pay attention that expression in the brackets is normal velocity $v_{\mathbf{n}}$ with some factor:

$$\left(\frac{\partial\Phi}{\partial z} - \frac{\partial\Phi}{\partial x}\frac{\partial\eta}{\partial x} - \frac{\partial\Phi}{\partial y}\frac{\partial\eta}{\partial y}\right)\bigg|_{z=\eta} = v_{\mathbf{n}}[1 + (\nabla\eta)^2],$$

and gives insight in the first (kinematic) boundary condition (3). You can see that this boundary condition requires that the surface has to move with the same velocity as the fluid.

As a first step let us take care of the second term. Using the definition of potential on the surface ψ one can get the following relations

$$\frac{\partial\psi}{\partial x} = \frac{\partial}{\partial x}\Phi(x,y,\eta(x,y)) = \frac{\partial\Phi}{\partial x}\bigg|_{z=\eta} + \frac{\partial\Phi}{\partial z}\bigg|_{z=\eta}\frac{\partial\eta}{\partial x},$$

$$\frac{\partial\psi}{\partial y} = \frac{\partial}{\partial y}\Phi(x,y,\eta(x,y)) = \frac{\partial\Phi}{\partial y}\bigg|_{z=\eta} + \frac{\partial\Phi}{\partial z}\bigg|_{z=\eta}\frac{\partial\eta}{\partial y}.$$

Using these relations we immediately get

$$\left(\frac{\partial\Phi}{\partial x}\frac{\partial\eta}{\partial x} + \frac{\partial\Phi}{\partial y}\frac{\partial\eta}{\partial y}\right)\bigg|_{z=\eta}$$

$$= \nabla\psi \cdot \nabla\eta - \frac{\partial\Phi}{\partial z}\bigg|_{z=\eta}(\nabla\eta)^2, \quad (10)$$

which after substitution of (10) into (9) yields

$$\begin{aligned} T &= \frac{1}{2}\int (\nabla\Phi)^2 \mathrm{d}V \\ &= \frac{1}{2}\int \Phi\left(\frac{\partial\Phi}{\partial z}[1 + (\nabla\eta)^2] - \nabla\psi \cdot \nabla\eta\right)\bigg|_{z=\eta} \mathrm{d}x\mathrm{d}y. \quad (11) \end{aligned}$$

Let us emphasize the fact that up to now all derivations are exact, we haven't used the weak nonlinearity in the system yet.

B. Expansion of kinetic energy in terms of steepness.

1. Steepness as a measure of nonlinearity in the system.

From observation it is known that in most of the interesting cases steepness (average slope) of the surface μ is of the order of the value 0.1 or lower. Average slope can be introduced in numerous ways. Here are just few of them:

- $\mu = \sqrt{\langle|\nabla\eta|^2\rangle}$.
- $\mu = \langle|\nabla\eta|\rangle$.
- $\mu = \sqrt{\langle\eta^2\rangle}k_p$.

Here $k_p = 2\pi/\lambda_p$ is wavenumber corresponding to the characteristic wavelength of the wave field λ_p. In terms of wavenumber Fourier spectrum of the wave field it is wavenumber of the peak of the spectrum. Because we shall be working with the weakly nonlinear wave field it is natural to use Fourier transform in xy-plane. Let's introduce it for function of two variable $f = f(x,y) = f_{\mathbf{r}}$:

$$\hat{F}[f_{\mathbf{r}}] = f_{\mathbf{k}} = \frac{1}{(2\pi)^2}\int f_{\mathbf{r}}e^{\mathrm{i}\mathbf{k}\mathbf{r}}\mathrm{d}^2r, \quad (12)$$

$$\hat{F}^{-1}[f_{\mathbf{k}}] = f_{\mathbf{r}} = \int f_{\mathbf{k}}e^{-\mathrm{i}\mathbf{k}\mathbf{r}}\mathrm{d}^2k. \quad (13)$$

For periodic boundary conditions, obviously, these Fourier integrals should be replaced by Fourier series. In the case of $2\pi \times 2\pi$ periodic box Fourier series and these Fourier integrals will coincide. Now let us try to get expansion of kinetic energy up to the quartic terms.

From the Laplace equation (1) after Fourier transform in xy-plane one gets equation

$$\frac{\partial^2\Phi_{\mathbf{k}}}{\partial z^2} - k^2\Phi_{\mathbf{k}} = 0,$$

which together with boundary conditions at infinite depth (solution has to decay for negative z) immediately yields

$$\Phi_{\mathbf{k}} = A_{\mathbf{k}}e^{kz}, \quad \frac{\partial\Phi_{\mathbf{k}}}{\partial z} = kA_{\mathbf{k}}e^{kz} = k\Phi_{\mathbf{k}}. \quad (14)$$

Here we introduced magnitude of the wavevector $k = |\mathbf{k}|$.

2. Expansion of potential at the surface.

Now let us express $A_{\mathbf{k}}$ through the functions on the surface. In order to do this we expand exponential function in (14) up to the second order terms:

$$\Phi_{\mathbf{k}} \simeq A_{\mathbf{k}}\left(1 + kz + \frac{1}{2}(kz)^2\right). \qquad (15)$$

Pay attention, that on the surface $z = \eta$ and kz is of the order of steepness μ, which is our small parameter. We limit ourselves by quadratic terms, because together with amplitude A they will give cubic term for Φ, while in the kinetic energy (11) derivative $\partial\Phi/\partial z$, which will be of the same order as Φ, is multiplied by potential Φ, which will result in quartic terms in Hamiltonian. Further expansion will give us higher order terms.

After inverse Fourier transform of (15) expanded potential takes the form

$$\Phi(x,y,z) = \hat{F}^{-1}[\Phi_{\mathbf{k}}] \simeq A(x,y)$$
$$+ z\hat{F}^{-1}[kA_{\mathbf{k}}] + \frac{z^2}{2}F^{-1}[k^2 A_{\mathbf{k}}],$$

which on the surface gives

$$\psi(x,y) = \Phi(x,y,z)|_{z=\eta} = A(x,y)$$
$$+ \eta\hat{F}^{-1}[kA_{\mathbf{k}}] + \frac{\eta^2}{2}F^{-1}[k^2 A_{\mathbf{k}}], \qquad (16)$$

here $A(x,y) = \hat{F}^{-1}[A_{\mathbf{k}}]$ and from now on we shall replace $\simeq$ sign with equality.

It is convenient to introduce linear nonlocal operator $\hat{k}$ in the following way:

$$\hat{k}f(x,y) = \hat{F}^{-1}[k\hat{F}[f_{\mathbf{r}}]] = \hat{F}^{-1}[kf_{\mathbf{k}}]. \qquad (17)$$

In other words, this operator acts as follows: it multiplies Fourier harmonics by the magnitude of corresponding wave number. Due to this property it is often referred as a square root of negative Laplacian: $\hat{k} = \sqrt{-\Delta}$. With this operator we get the following compact notation:

$$\psi(x,y) = A + \eta\hat{k}A - \frac{\eta^2}{2}\Delta A, \qquad (18)$$

In order to calculate $\partial\Phi/\partial z$ on the surface, according to (14) we need to find A. Let us write equation for A:

$$A = \psi - \eta\hat{k}A + \frac{\eta^2}{2}\Delta A, \qquad (19)$$

this is integro-differential nonlocal equation. Let us solve it by iterations, keeping terms up to cubic ones. In the first iteration we put $A = \psi$ in the right hand side of (19):

$$A = \psi - \eta\hat{k}\psi + \frac{\eta^2}{2}\Delta\psi. \qquad (20)$$

In the second iteration we substitute this result (20) in the right hand side of (19) (omit terms higher than cubic ones):

$$A = \psi - \eta\hat{k}\psi + \frac{\eta^2}{2}\Delta\psi + \eta\hat{k}[\eta\hat{k}\psi]. \qquad (21)$$

This is our solution with desired accuracy. Now we can use it for $\partial\Phi/\partial z$ on the surface.

3. Expansion of $\partial\Phi/\partial z$ at the surface.

Let us apply exactly the same approach to the z-derivative of potential. From (14) and (15) one gets (up to the cubic terms):

$$\frac{\partial\Phi_{\mathbf{k}}}{\partial z}(x,y,z) \simeq kA_{\mathbf{k}}\left(1 + kz + \frac{1}{2}(kz)^2\right). \qquad (22)$$

After the inverse Fourier transform:

$$\frac{\partial\hat{F}^{-1}[\Phi_{\mathbf{k}}]}{\partial z} \simeq \hat{F}^{-1}[kA_{\mathbf{k}}] + z\hat{F}^{-1}[k^2 A_{\mathbf{k}}] + \frac{z^2}{2}F^{-1}[k^3 A_{\mathbf{k}}],$$

which on the surface gives

$$\frac{\partial\Phi}{\partial z}\bigg|_{z=\eta} = \hat{F}^{-1}[kA_{\mathbf{k}}] + \eta\hat{F}^{-1}[k^2 A_{\mathbf{k}}] + \frac{\eta^2}{2}F^{-1}[k^3 A_{\mathbf{k}}].$$

This expression can be rewritten using $\hat{k}$-operator:

$$\frac{\partial\Phi}{\partial z}\bigg|_{z=\eta} = \hat{k}A - \eta\Delta A - \frac{\eta^2}{2}\Delta[\hat{k}A]. \qquad (23)$$

Let us substitute here A from expression (21) and keep only terms up to cubic ones:

$$\frac{\partial\Phi}{\partial z}\bigg|_{z=\eta} = \hat{k}\psi - \eta\Delta\psi - \frac{1}{2}\eta^2\Delta\hat{k}\psi - \hat{k}[\eta\hat{k}\psi]$$
$$+ \eta\Delta(\eta\hat{k}\psi) + \frac{1}{2}\hat{k}[\eta^2\Delta\psi] + \hat{k}[\eta\hat{k}[\eta\hat{k}\psi]]. \qquad (24)$$

Now we have everything for rewriting Hamiltonian in terms of η and ψ.

C. Weakly nonlinear Hamiltonian equations.

For given boundary conditions the following relation holds:

$$\int \eta\nabla\psi\mathrm{d}^2 r = -\int \psi\nabla\eta\mathrm{d}^2 r. \qquad (25)$$

For operator $\hat{k}$ we can derive similar relation:

$$\int \psi\hat{k}\eta\mathrm{d}^2 r = \int k\eta_{\mathbf{k}}\psi_{\mathbf{k}}^*\mathrm{d}^2 k = \int(\hat{k}\psi)\eta\mathrm{d}^2 r, \qquad (26)$$

where we used the relation for Fourier image of a real valued function $\psi_{-\mathbf{k}} = \psi_{\mathbf{k}}^*$, while $*$ means complex conjugation.

Using (25)-(26) and (24) kinetic energy (11) can be written in a relatively compact form:

$$T = \frac{1}{2}\int \psi\hat{k}\psi\mathrm{d}^2r + \frac{1}{2}\int \eta\left[|\nabla\psi|^2 - (\hat{k}\psi)^2\right]\mathrm{d}^2r$$
$$+ \frac{1}{2}\int \eta(\hat{k}\psi)\left[\hat{k}(\eta(\hat{k}\psi)) + \eta\nabla^2\psi\right]\mathrm{d}^2r. \quad (27)$$

Because we expand Hamiltonian up to quartic terms using small parameter $\mu \approx |\nabla\eta| \approx |\hat{k}\eta|$ one can expand part of potential energy associated with capillary waves:

$$\sigma'\left(\sqrt{1+|\nabla\eta|^2} - 1\right) \simeq \sigma'\left(\frac{1}{2}|\nabla\eta|^2 - \frac{1}{8}|\nabla\eta|^4\right). \quad (28)$$

Hamiltonian, resulting from (6), (28), and (27) have the following form

$$H = \frac{1}{2}\int \left(\sigma'|\nabla\eta|^2 + g\eta^2 + \psi\hat{k}\psi\right)\mathrm{d}^2r$$
$$+ \frac{1}{2}\int \eta\left[|\nabla\psi|^2 - (\hat{k}\psi)^2\right]\mathrm{d}^2r$$
$$+ \frac{1}{2}\int \eta(\hat{k}\psi)\left[\hat{k}(\eta(\hat{k}\psi)) + \eta\nabla^2\psi\right]\mathrm{d}^2r$$
$$- \frac{1}{8}\int \sigma'|\nabla\eta|^4\mathrm{d}^2r. \quad (29)$$

Hamiltonian equations (7) can be written as follows

$$\dot{\eta} = \hat{k}\psi - (\nabla\cdot(\eta\nabla\psi)) - \hat{k}[\eta\hat{k}\psi] + \hat{k}(\eta\hat{k}[\eta\hat{k}\psi])$$
$$+ \frac{1}{2}\nabla^2[\eta^2\hat{k}\psi] + \frac{1}{2}\hat{k}[\eta^2\nabla^2\psi],$$
$$\dot{\psi} = \sigma'\nabla^2\eta - g\eta - \frac{1}{2}\left[|\nabla\psi|^2 - (\hat{k}\psi)^2\right]$$
$$- [\hat{k}\psi]\hat{k}[\eta\hat{k}\psi] - [\eta\hat{k}\psi]\nabla^2\psi - \frac{1}{2}\sigma'\nabla\cdot(|\nabla\eta|^2\nabla\eta). \quad (30)$$

In many cases, when capillary waves are considered it is enough to limit ourselves by cubic terms in the Hamiltonian, this is why the quartic capillary term is often dropped even when capillary effects are taken into account.

II. DEPENDENCE OF THE CONSTANT OF THE SPECTRUM ON FORCING AMPLITUDE.

KZ finite flux of wave action solution corresponding to inverse cascade is (see main paper):

$$n_k^{(2)} = C_2 Q^{1/3} k^{-23/6},$$

here C_2 is some constant and Q is the magnitude of wave action flux. The value of the constant C_2 is unknown,

while Q depends on the strength of pumping. If we assume that in spite of finiteness of both inertial intervals (for inverse and direct cascades) all pumped in wave action has to be transferred by inverse cascade, it would mean that Q is proportional to the rate of injection of the wave action. Let us try to evaluate how it depends on the only changing parameter of the pumping F_0 (amplitude of pumping, was increased in different simulations by a factor of $\times 2$, $\times 4$, and $\times 8$, which resulted in increase of average steepness) in a linear approximation (the system is weakly nonlinear, so it is reasonable for the first approach to the problem). For the pumping region $k \in [k_{p1}, k_{p2}]$ we have the following linear equation:

$$\dot{a}_\mathbf{k} = -\mathrm{i}\omega_k a_\mathbf{k} + \ldots + F_0 p(k)\mathrm{e}^{iR_\mathbf{k}(t)},$$
$$p(k) = 4\sqrt{\frac{k}{2\omega_k}}\frac{(k-k_{p1})(k_{p2}-k)}{(k_{p2}-k_{p1})^2}, \quad (31)$$

where $R_\mathbf{k}(t)$ is a uniformly distributed random number in interval $(0, 2\pi]$. Integrating this linear equation one can get:

$$a_\mathbf{k}(t) = F_0 a_k(0)\mathrm{i}p(k)\mathrm{e}^{-\mathrm{i}\omega_k t}\int_0^t \mathrm{e}^{\mathrm{i}(R_k(\tau)+\omega_k\tau)}\mathrm{d}\tau. \quad (32)$$

We designed the experiment (and paid a very high price for that, decreasing the dynamic range of the inverse cascade by a factor of 2) in such a way, that only the third harmonic of pumping is reaching the dissipation region, meaning that we can neglect nonlinear drain of wave action from the pumping region through a decay of the third harmonic at least in the first approximation. Also, as was mentioned above, we suppose that almost all wave action injected into the system is gone by the inverse cascade. Then $n_\mathbf{k} \sim F_0^2 G(t, \mathbf{k})$, were G is some function of time and $\mathbf{k}$, and the rate of change of $N = \int n_\mathbf{k}\mathrm{d}\mathbf{k}$ is also proportional to F_0^2. In other words, using the lowest steepness (the smallest F_0) case as the reference (let us denote corresponding value of a flux as Q_1), we are expecting the wave action flux for other simulation to be $2^2 Q_1$, $4^2 Q_1$, and $8^2 Q_1$, which leads to changing the constant in front of the k-dependent part of the spectrum by factors of $2^{2/3}$, $4^{2/3}$, and $8^{2/3}$, if the formula for KZ-spectrum is correct. Let us compare this prediction with the observations. We used the least squares fit with $k^{-3.07}$ (the best common slope for all four simulations) and considered relative (with respect to $\mu = 0.054$ case) growth factor (GF) of the constant. Pay attention to the fact, that when we divide constants for different cases, the only unknown parameter C_2 cancels out. The results are given in Table I.

One can notice reasonable correspondence of expected growth factors and the measured ones taking into account simplicity of our model. Can one fit this data with a different dependence (power of Q)? Sure, e.g. if we consider the case when the constant in the spectrum depends on the wave action flux as $Q^{3/8}$, the expected grow factors

μ	Measured GF	Expected (2/3)	Error (2/3)
0.054	1	1	0%
0.067	1.593	1.587	0.328%
0.093	2.230	2.520	−11.5%
0.135	4.833	4	20.8%

TABLE I. Spectrum constant growth factors (with respect to $\mu = 0.054$ case) and their relative errors (measured-expected)/expected, where expected growth factors are $2^{2/3}$, $4^{2/3}$, and $8^{2/3}$, following from $Q^{1/3}$ dependence of the constant in the KZ-spectrum.

μ	Measured GF	Expected (3/4)	Error (3/4)
0.054	1	1	0%
0.067	1.593	1.682	−5.30%
0.093	2.230	2.828	−21.2%
0.135	4.833	4.757	1.60%

TABLE II. Spectrum constant growth factors (with respect to $\mu = 0.054$ case) and their relative errors (measured-expected)/expected, where expected growth factors are $2^{3/4}$, $4^{3/4}$, and $8^{3/4}$, following from hypothetical $Q^{3/8}$ dependence of the constant in the spectrum.

would be $2^{3/4}$, $4^{3/4}$, and $8^{3/4}$ and we could get much better correspondence for the highest nonlinearity (and only for that case!), as it is demonstrated in Table II.

Meanwhile, the magnitude of an error is growing in the first case (for $Q^{1/3}$) and behaves randomly in the second case (for hypothetic $Q^{3/8}$). Our linear analysis has to give higher and higher error with increase of nonlinearity and this is what we observe for the case of expected dependence $Q^{1/3}$ (like in KZ-spectrum), which means that

our measurements support this case in contrary to hypothetical $Q^{3/8}$ dependence.

III. DESCRIPTION OF FILES WITH INFORMATION ABOUT THE SURFACES OF η AND ψ.

In order to provide a reader with a possibility to investigate different characteristics of the wave field in all simulations reported in the paper, the files of surfaces of $\eta(\mathbf{r})$ and $\psi(\mathbf{r})$ are given in Supplemental Materials as a downloadable archive eta_psi_surfaces.zip. Every file is named according to its content. For example, the file eta_r.mu_0.054_time_1.126222214538720e+06.data contains information about $\eta(\mathbf{r})$ surface for the simulation with average final steepness $\mu \approx 0.054$ at the final moment of time $t = 1.126222214538720 \times 10^6$. The file psi_r.mu_0.135_time_7.907737882729195e+05.data contains information about $\psi(\mathbf{r})$ surface for the simulation with average final steepness $\mu \approx 0.135$ at the final moment of time $t = 0.7907737882729195 \times 10^6$. Every file contains ASCII text in the following format: the first two columns are x and y coordinates, the third column is the value of $\eta(\mathbf{r})$ or $\psi(\mathbf{r})$ in a given point of the surface. There is an empty line between changes of the first ("slow") coordinate. The format is ready for plotting as a 3D-surface by standard scientific visualization tools like Gnuplot or Octave. The grid is homogeneous, resolution is 512×512 points, size of the domain is $2\pi \times 2\pi$. Due to periodic boundary conditions the coordinates are changing in an interval $0 \leq x, y < 2\pi$ and the coordinates grid step is $2\pi/512$. The choice of $\mathbf{r}$-representation was natural, as scaling of amplitudes of the $\mathbf{k}$-representation would depend on a definition of the Fourier transformation.

[1] V. E. Zakharov, J. Appl. Mech. Tech. Phys. **9**, 190 (1968).